

June 2020

Treball Final del
Grau en Enginyeria Física

On the optimisation of Single Molecule Localization Microscopy using Deep Learning

Aida Perramon Malavez

Coordinator at TU Delft: Bernd Rieger

Coordinator at UPC: Clara Prats Soler

Technische Universiteit Delft
Delft, The Netherlands



List of contents

Abstract.....	2
Acknowledgements	3
1. Introduction	4
1.1. History of microscopy	4
1.2. Localization microscopy	5
1.3. Statistics in Localization microscopy	7
1.4. Social context	8
1.5. Objectives	9
1.6. Outline	9
2. Method to improve super resolution: Evaluation	10
2.1. Implementation of MINFLUX	10
2.2. Examining the potential of the method	13
2.2.1. Rhombic pattern.....	13
2.2.2. Parameters study	15
2.2.3. Shrinkage of the PSF area.....	20
2.2.4. Illumination beam: Parabolic shape	21
2.2.5. Illumination beam: Gaussian shape	23
2.3. Deep Learning – Functions for MINFLUX	25
2.4. Deep Learning – Learned Mask	26
2.4.1. Changes in parameter_settings_demo4.py.....	29
2.4.2. Changes in data_utils.py	30
2.4.3. Changes in physics_utils.py.....	30
2.4.4. Changes in loss_utils.py.....	30
2.4.5. Changes in cnn_utils.py	31
3. Further discussion.....	32
4. Conclusions and perspectives.....	34
Bibliography	36
Annex	38

Abstract

The greatest advances in the biomedical field would not have been possible without microscopy. The higher the resolution of the image obtained, the more details one can know about the sample. In the last few decades, microscopy have progressed from differentiating objects at millimetres of distance to the nanoscale.

The latter accuracy is achieved using the contemporary super resolution microscopy, including Single Molecule Localization Microscopy, examples of which are the fluorescence microscopy techniques PALM and STORM. This kind of imaging method is done by stochastically activating and deactivating a set of fluorescent molecules distributed in a sample, taking a picture of it with a CCD camera in every switch, and then processing all the frames to obtain a final image.

However, nowadays precision is of tens of nanometres, which suggests that there is still room for improvement. Furthermore, the state-of-the-art super resolution techniques still exhibit certain drawbacks such as overlapping between emitters PSFs and the difficulty to make molecular tracking especially due to photobleaching.

Therefore, some techniques have recently been developed to improve super resolution microscopy, such as MINFLUX and DeepSTORM. MINFLUX aims to minimize the number of emitted photons required for the localization of molecules with the main objective of being able to do molecular tracking, while DeepSTORM focuses on eliminating the overlapping of PSFs using a Deep Learning algorithm to create a phase mask that generates a suitable PSF for this purpose.

In this project both techniques are to be combined expecting to obtain highly accurate estimations of the emitters' two-dimensional positions with resolutions of units of nanometres, while avoiding overlapping of PSFs in highly dense samples and minimizing the number of photons emitted per fluorophore.

Acknowledgements

The realisation of this project has not only challenged myself in many ways, but also the relationship with my significant others. To all of you that have given me support when I needed it, stood by me when the stress was overwhelming and that have listened to my complaints when things got hard, thank you. Especially to my beloved housemates, Den Hoek felt like family, without your hospitality and kindness the experience of living abroad would have been as hard as riding a bike against the wind of the second weekend of February.

However, my most sincere appreciation is to professor Bernd Rieger without whom this project would not have even started. Thank you for letting me learn from you and the colleagues of the department of Imaging Physics of the TU Delft, for showing me what it really means to do research, for your dedication, patience and kindness, which made it easier to carry out this thesis. Moreover, I would like to thank Rasmus Ø. Thorsen for, despite having to work on his PhD and supervise other students, helping me with the project either with MATLAB codes, tricky concepts, bad results or moral support.

Special thanks to Elias Nehme for his help with the DeepSTORM Deep Learning code. Without being his responsibility, he kindly guided me through it.

Furthermore, I would like to thank Ronald Ligteringen for his hospitality, kindness and help with different informatic problems, in particular with connecting to the servers of the University remotely, for which I am very grateful because it allowed me to continue the thesis when because of the Coronavirus pandemic I had to return to Barcelona.

Not to forget my workmates Ewout, Teun, Natalie, Valentino and Joris, I wish we got to spend more time together, thank you for your constant cheerfulness and help, it definitely pushed me to work harder and better. And also thank you to my dear friend Inma Villanueva, for being always there, either to talk and evade or to share ideas and help to put them in practice.

To my incredibly talented friends the PhD student Martí Català and Gerard Pons, I would like to say thank you for your support, scientific and programming help and your constant encouragement. Also, the professor Clara Prats deserves my most sincere thanks for having accepted to be my supervisor and for having been available whenever I have needed her, despite the many other projects she tutorises and the huge amount of work the Coronavirus pandemic has caused her and the other COMBIO research group members.

Thank you, family, friends, colleagues, professors. Without all of you, getting to live this experience and fulfil my objectives in my academic career would have been impossible.

Moltes gràcies. Heel erg bedankt.

1. Introduction

1.1. History of microscopy

The global pandemic caused by the COVID-19 virus has led to the need to swiftly investigate and learn about biological agents, once again demonstrating the importance of microscopy and to improve the resolution of the existent optical microscopes by developing new super resolution techniques.

Indeed, if it were not for the invention and progress of microscopy, the greatest advances and discoveries in the medical and biological fields among others, could not have been possible. Anton van Leeuwenhoek from Delft, Holland, often named the father of microscopy, is to owe for that because he invented in the 17th century the first, small and simple microscope. It was made of only a single lens with a magnification of up to 270 x, allowing him to observe, for the first time, cells and bacteria.

But it was not until the 19th century when real technological advances emerged, specially thanks to the work of Joseph von Fraunhofer to correct chromatic aberrations and Carl Zeiss setting up his own business with the goal of creating high-quality research instruments.

Thus, conventional microscopy such as wide-field transmission microscopy or others using compound and simple microscopes was born [1]. And when Dr. Ernest Abbe started to work for Zeiss, he formulated his wave theory of microscopic imaging and defined what is now known as Abbe's diffraction limit. The diffraction limit originates from the wave nature of light [2], entailing that the numerical aperture (NA) of the objective lens has to be large enough to have, at the intermediate image plane, the first-order diffraction pattern produced by the sample at the wavelength λ of the incident illumination. **Figure 1.1.** shows a schematic of that proposition.

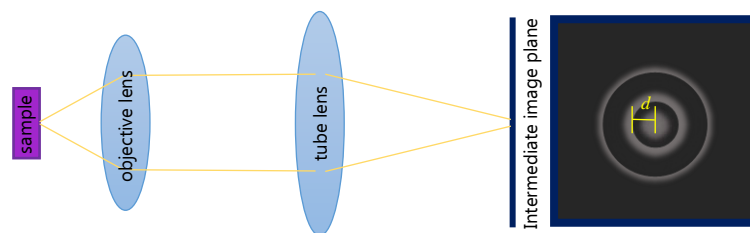


Figure 1.1. Scheme of a simple microscope and diffraction pattern formed in the intermediate image plane. Distance d indicates the diffraction-limited resolution.

Hence, Ernest Abbe claimed that objects closer than a distance

$$d = \frac{\lambda}{2 NA} \quad (1.1.)$$

cannot be discerned. For the highest immersion oil NA lenses and visible light, that distance d is at best 200 nm [3].

However, super resolution methods that have been developed in recent years such as photoactivated localization microscopy (PALM) and stochastic optical reconstruction microscopy (STORM) allow nanoscale visualisation of biological agents. These two techniques use fluorescence localization based on the stochastic on and off switching of fluorescent emitters in the sample. The resolution is now limited by the localization precision and the density of fluorophores, not any longer by the diffraction limit [4].

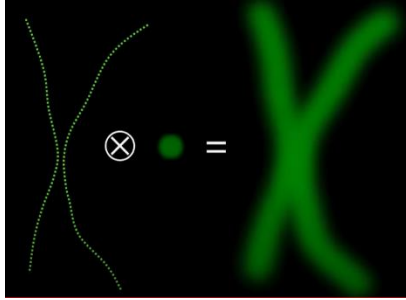


Figure 1.2. Scheme of imaging with a microscope, the final image is the convolution of the object and the PSF of the system [6].

The images taken by the aforementioned microscopy techniques, used to recover the position of the fluorescent molecules in the sample, show the convolution of the object (the fluorophore) and the point-spread function (PSF) of the optical system when incoherent illumination is used, i.e. the microscope does not transform a point in the object space into a point in the image plane but what you get is a diffraction figure which is the PSF, as in the case shown in **Figure 1.2**. The PSF describes the impulse response of the system to a point-like sample, occupying a volume in space because it has an extension in the transverse plane and also in the axial direction [5].

In **Figure 1.1**, the diffraction pattern in the intermediate image plane, also known as Fourier plane, would correspond to the PSF if the sample was an ideal point-like source.

When in the object plane you have a sample formed by a set of points, in the image plane you will have the convolution of this object with the PSF of the system:

$$I(x, y) = o(x, y) \times h(x, y) + N(x, y), \quad (1.2.)$$

where $I(x, y)$ represents the intensity distribution of the image, $o(x, y)$ states for the intensity function of the object, $h(x, y)$ is the intensity function of the PSF and $N(x, y)$ represents the background noise of the system [7], [8].

Therefore, to have a good image a convenient solution is to decrease the footprint of the PSF by, for example, increasing the NA of the lenses and decreasing the wavelength of the illumination.

1.2. Localization microscopy

The state-of-the-art localization microscopy consists of processing a set of camera images (10^3 – 10^6 frames) of the sample while fluorophores stochastically activate and deactivate. Each frame shows many point-spread functions of the active emitters in the field of view (FOV) appearing as blurry spots that can sometimes overlap, as seen in **Figure 1.3**.

For each frame, the position of the emitters can be accurately recovered by fitting a PSF model to the data. This results in an image of the sample in which the diffraction limit has been overcome [9], [10].

Nevertheless, if the frame consists of overlapping PSFs, recovering the position of the emitter from the images can be arduous, getting a high number of false position estimations.

Next to the established Single Molecule Localization Microscopy (SMLM) methods like PALM and STORM, new techniques are being developed in order to increase the resolution or allow image a densely labelled sample in a short time (in 3D), such as MINFLUX [11] and DeepSTORM [10] which will be adopted in this project.

MINFLUX was created with the objective to increase the resolution while reducing the number of required collected photons. In MINFLUX, the sample is illuminated with a donut-shaped beam in four different positions, three of them forming an equilateral triangle and the other one being the centroid of the latter. From the different number of photons obtained at each position, i.e., the different photon counts n_i with $i \in \{0, K - 1\}$ being K the number of different detections ($K = 4$ in this case), the location of the emitter is estimated using a maximum likelihood estimator (MLE). However, the technique has some disadvantages, as for a large FOV this is a very slow technique. Besides, the four positions must be already close to the location of the emitter (within the diffraction limit) to improve over standard SMLM.

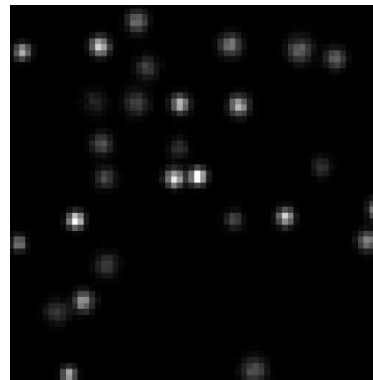


Figure 1.3. Simulated camera detection of the emission of active fluorophores during a SMLM experiment, using the Thunder-STORM plugin for ImageJ developed by Nehme, E. *et al.* [10].

DeepSTORM is a possible solution to overlapping PSFs due to many active emitters per frame for 2D and specially 3D imaging [12]. It is a method of PSF engineering that learns via Deep Learning to generate a phase mask. This mask is introduced with a Spatial Light Modulator (SLM) to the imaging path [13] of the optical system and is programmed so that the PSF shape of the system changes with the axial position while having an as small as possible footprint in the image to avoid overlapping. DeepSTORM3D operates using a Convolutional Neural Network (CNN) for analysing the sample in regions where PSFs overlap. It uses an engineered PSF that is designed optimally for 3D localization over an axial range of $4 \mu\text{m}$.

When a physical-simulation layer with an adjustable phase modulation is added to the CNN, it is possible to learn the optimal PSF for its purpose and the associated localization algorithm.

1.3. Statistics in localization microscopy

In order to evaluate the precision of the proposed measurement scheme in MINFLUX, the Cramer–Rao Low Bound (CRB/CRLB) has to be calculated. For that, one has to compute the Fisher information that the photon counts n_i collected in an experiment hold of the fluorophore’s location. The number of photon counts are the result of multiplying the total number of photons emitted (N) by the intensity detections I_i for every exposure of the emitter.

Those n_i follow a Poissonian distribution with mean λ_i , i.e. $P(n_i) \sim \text{Poisson}(\lambda_i)$:

$$\lambda_i = c_e q_e \sigma_a I_i(\bar{r}), \quad (1.3.)$$

where c_e is the collection efficiency of the system, q_e its quantum yield and σ_a the absorption cross–section of the emitter at the illumination’s wavelength.

For an easier analysis, one can compute the probabilities for n_i conditioned to N , yielding to multinomial statistics, i.e. $P(\bar{n}|N) \sim \text{Multinomial}(\bar{p}|N)$, being \bar{p} the parameter vector:

$$P(\bar{n}|N) = \frac{N!}{n_0! \dots n_{K-1}!} \prod_{i=0}^{K-1} p_i^{n_i}, \quad (1.4.)$$

$$p_i(\bar{r}) = \frac{\lambda_i}{\sum_{j=0}^{K-1} \lambda_j} \text{ with } i \in \{0, K-1\}. \quad (1.5.)$$

In **equations 1.3.** and **1.5.**, \bar{r} is the position of the fluorophore.

The Fisher matrix $F_{\bar{r}}$ has to be calculated to measure the information that the n_i hold on the emitter position \bar{r} , which belongs to the d –dimensional space, $\bar{r} = [r_1 \dots r_d]^T$. This can be done more easily if the Fisher information matrix for \bar{p} , $F_{\bar{p}}$, is computed first, because it can be obtained more directly. Then the reparameterization:

$$F_{\bar{r}} = \mathcal{J}^T F_{\bar{p}} \mathcal{J} \quad (1.6.)$$

is used, where

$$\{F_{\bar{p}}\}_{ij} = N \left(\frac{1}{p_{K-1}} + \frac{\delta_{ij}}{p_i} \right) \text{ with } i, j \in \{0, K-2\}. \quad (1.7.)$$

δ_{ij} is the Kronecker delta function and $\mathcal{J} \in \mathbb{R}^{(K-1) \times d}$ is the Jacobian matrix of the transformation from the \bar{r} –space to the \bar{p} –space where $i \in \{0, K-2\}$, and therefore:

$$\mathcal{J} = \begin{bmatrix} \frac{\partial p_0}{\partial r_1} & \dots & \frac{\partial p_0}{\partial r_d} \\ \vdots & \ddots & \vdots \\ \frac{\partial p_{K-2}}{\partial r_1} & \dots & \frac{\partial p_{K-2}}{\partial r_d} \end{bmatrix}. \quad (1.8.)$$

Once the Fisher information matrix is obtained, a lower bound for the covariance matrix of the fluorophore position ($\text{Covar}(\bar{r})$) can be derived from the Cramer–Rao inequality:

$$\text{Covar}(\bar{r}) \geq \text{Covar}_{CRB}(\bar{r}) = F_{\bar{r}}^{-1}. \quad (1.9.)$$

Consequently, the mean Cramer–Rao Low Bound (CRLB) is:

$$\tilde{\sigma}_{CRLB} = \sqrt{\frac{\text{tr}(\text{Covar}_{CRB})}{d}}. \quad (1.10.)$$

For the purpose of estimating the location \hat{r} of a fluorophore, however, in SMLM with MINFLUX a position estimator is needed, for example an MLE, that is defined as:

$$\hat{r}_{MLE} = \text{argmax } \mathcal{L}(\bar{r}|\bar{n}), \quad (1.11.)$$

where $\mathcal{L}(\bar{r}|\bar{n})$ is the likelihood function dependent on the probability distribution defined in [equation 1.4.](#), and to obtain the estimator one has to maximize the log-likelihood function.

Thus, in order to estimate the 2D position of the emitter with the four donut-shaped beams already mentioned in [section 1.2.](#), one has to maximize numerically:

$$\ln \mathcal{L}(\bar{r}|\bar{n}) \propto \ell(\bar{r}|\bar{n}) = \sum_{i=0}^{K-1} n_i \ln(p_i), \quad (1.12.)$$

where a simplified likelihood function $\ell(\bar{r}|\bar{n})$ is defined using [equation 1.4.](#)

Other estimators can be used, such as a least mean square estimator (LMSE) or a numerically unbiased LMSE [11]. In addition, one can also modify this methodology to make a 3D position estimation and recover also the axial position of the molecule. In the simulations carried out in this thesis, only 2D localization will be considered.

1.4. Social context

It is important to notice that this project has been developed under extraordinary circumstances. The global crisis that started in February 2020 due to the coronavirus (COVID-19) pandemic has affected our lives in ways we could not have imagined. A serve number of deaths, the anxiety and desperation of confronting the unknown, the lack of medical resources, the lockdowns, ... are important factors to take into account in order to acknowledge the work behind the thesis. By cause of the lockdown policies adopted by the majority of worldwide governments, remote working and online classes have been accepted as alternatives to the previous normality. This may cause learning difficulties, because it makes it more difficult to contact (and stay in contact) with supervisors and professors, in addition to forcing us to re-educate ourselves in other ways of working and learning. Also, I started this project in the Netherlands, in the Technical University of Delft, granted with an Erasmus + apprenticeship, but due to the exceptional circumstances I had to go back to Barcelona and work remotely from another country with more restrictive policies than the country of destination, thus generating an imbalance between will and possibility. The objectives proposed originally with respect to the Deep Learning have had to be reconsidered since the difficulty of access to support has made it impossible to create an analytical model of the PSF.

1.5. Objectives

The main objective of this thesis is to optimize the Single Molecule Localization Microscopy (SMLM) performance.

Specific objectives

- To understand MINFLUX [11] and determine its efficiency.
- To research whether or not the MINFLUX method can be improved manually by changing the setup established.
- To research whether or not the MINFLUX method can be improved manually by changing the set parameters.
- To explore the possibility of performing MINFLUX with a parabolic or Gaussian beam shape rather than the donut.
- To optimise the shape of the beam used in MINFLUX with a Deep Learning algorithm, minimizing the footprint of the PSF of the system.
- To understand the Deep Learning code developed by Nehme, E. *et al.* [12] and adapt it to MINFLUX requirements.
- To use the phase mask obtained with the Deep Learning code to generate a PSF that can be used in the MINFLUX method improving its performance.

1.6. Outline

In the second section of this thesis the research procedure will be detailed. Briefly, a MATLAB code has been generated to do a statistical analysis of the performance of different approaches to MINFLUX. Then, a code in order to compute the area of certain PSFs and one to obtain the CRLB from the Fisher information matrix has been programmed. An area-optimisation algorithm has been introduced in the Deep Learning code developed by Nehme, E. *et al.* [12]. An adaptation of all functions comprising the aforementioned Deep Learning algorithm has been done with the aim of introducing the MINFLUX methodology in it and generating a mask for the illumination in 2D instead of three-dimensions. The results obtained will be then discussed and conclusions will be extracted.

2. Method to improve super resolution: Evaluation

With the aim of implementing the MINFLUX technique into the Deep Learning code created by Nehme, E. *et al.* [12], the first approach to be taken is to reproduce the method with a MATLAB algorithm and perform several testing in order to research the key parameters and the possibility of improvement of the method. Once familiarization with MINFLUX is gained, the Deep Learning code will be studied and adapted to obtain a phase mask that can modify the PSF of the system for a better performance of SMLM.

2.1. Implementation of MINFLUX

First of all, the theory of the MINFLUX technique has to be implemented into a MATLAB code, that can be found in the [Annex](#) of this thesis, in order to control the method.

MINFLUX purpose is to use an illumination intensity near to zero to excite the fluorescent molecules, modelled as point-like emitters. However, to find their location, the intensity profile should not be uniform, but have a minimum. Thus, the photon counts obtained when illuminating an emitter will depend on the proximity of the minimum of the illumination intensity to the molecule, tending to zero when they correspond. Therefore, the key in MINFLUX is the illumination beam shape or pattern. It is proven [11] that a donut-shaped beam has a very good performance in this methodology. The CRLB is reduced compared to flat-field illumination.

In MINFLUX, illumination is done four times, changing the beam position as in the vertex of an equilateral triangle and its centroid, as shown in [Figure 2.1](#). The displacement of the beams (L), i.e., the diameter of the circumference that forms the vertices of the triangle formed by the different beam positions, is an important parameter to be taken into account.

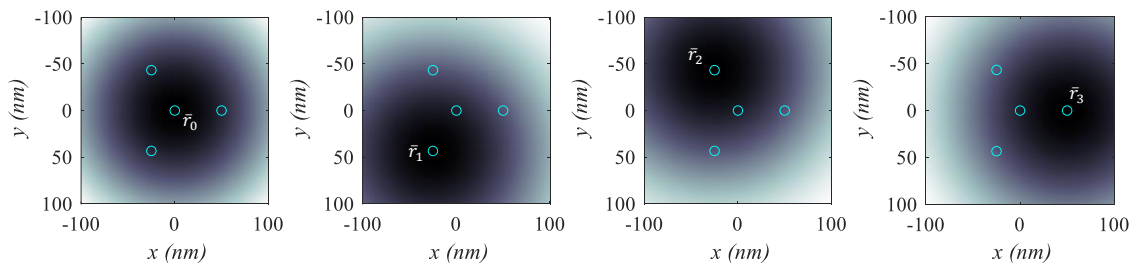


Figure 2.1. Scheme of the different beam positions in an experiment using MINFLUX. The location of the beams depends on the location of the target emitter, that should be comprised within the circumference formed by the position of the beams.

Reducing it diminishes the probability of overlapping and therefore exciting other molecules, which would make the localization of the emitter erratic. The scan region defined by parameter L must be smaller than the diffraction limit, but at the same time the circumference has to contain the molecule, which location has to be found or approximated before performing the experiment. Thus, one could start with a higher value of L and decrease it iteratively.

A brief description of the physics behind localization microscopy, introducing the concept of PSF, can be found in [sections 1.1.](#) and [1.2.](#) of this thesis. The illumination intensity will follow the donut profile:

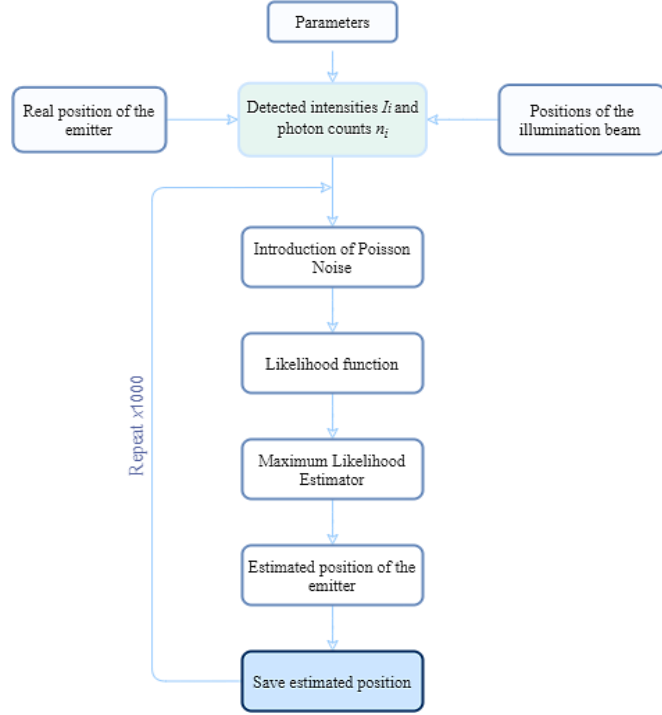


Figure 2.2. Flowchart describing the computation of an MLE while using the MINFLUX method.

$$I_{donut} = A_0 4e \ln 2 \frac{r^2}{fwhm^2} e^{-4 \ln 2 \frac{r^2}{fwhm^2}}, \quad (2.1.)$$

where A_0 is a normalization constant, $fwhm$ is a size-related parameter for the donut and

$$r = (\bar{r}_{emitter} - \bar{r}_{beam_i}) \quad (2.2.)$$

for $i \in \{0, K - 1\}$ with $K = 4$ the total number of different positions for the illumination beams, thus leading to the four percentages:

$$\%_i = \frac{I_{donut_i}}{\sum_{i=0}^3 I_{donut_i}}. \quad (2.3.)$$

When the percentage is multiplied by the total number of photons (N), one gets the photon counts n_i for the different exposures of the emitter.

Following the steps described in [section 1.3.](#), a Maximum Likelihood Estimator is programmed with the aim of recovering the position of the simulated emitter. The MLE is computed for 1000 different Poisson noise (λ_b) additions to simulate a real experiment which will surely obtain a noisy measurement due to instrumental limitations. A vector that contains the 1000 estimated positions of the active fluorophore is therefore obtained.

Implementing this process into a MATLAB code, which **Figure 2.2.** describes, one can simulate a localization microscopy experiment using MINFLUX, the results of which can be seen in **Figure 2.3.**

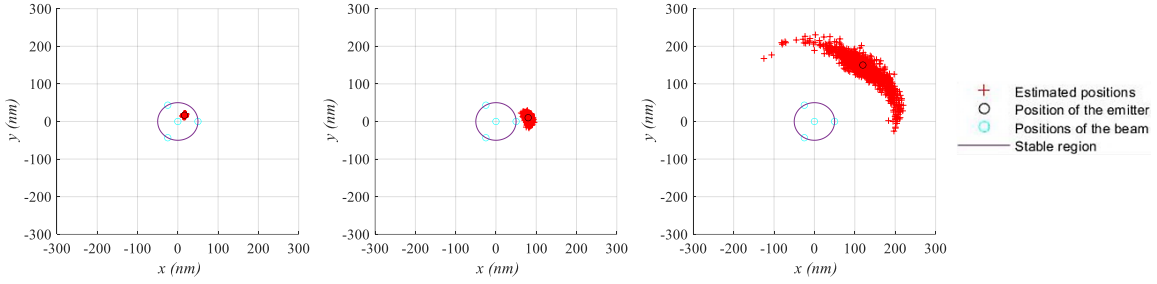


Figure 2.3. Estimation of the position of the emitter in a SMLM simulation using an MLE as described in the MINFLUX technique, for three different positions of the fluorophore. It can be seen that the circumference formed by the vertices of the equilateral triangle constituted by the different beam positions surrounds the convergence region of the method.

In **Figure 2.3.** it is shown a localization experiment for an emitter located at (16.7, 16.7) nm, (80, 10) nm and (120, 150) nm, respectively. The estimation of the position gets more erratic the more distance between the location of the emitter and the region within the circumference formed by the vertices of the equilateral triangle of beam positions, inducing to consider that region as of convergence.

Turning this code into a function and performing the same analysis for the different emitter positions possible in a lattice 50 x 50, with axis going from -60 to 60 nm in the x and y directions, the matrixes of the Standard Deviation (STD) and Root Mean Square Error (RMSE) of this method can be calculated using the saved 1000 location estimations for each iteration, as follows:

$$Absolute\ Error\ (AE) = |\bar{r}_{MLE} - \bar{r}_{emitter}|, \quad (2.4.)$$

$$RMSE = \frac{\sqrt{\sum_{t=1}^T AE_t^2}}{T}, \quad (2.5.)$$

with T the total number of repetitions of the process, i.e., 2500 in the case of study. The STD is directly computed with a MATLAB auxiliary function *std()*, obtaining the standard deviation of the different estimated positions for each emitter possible location in the lattice, separating its components x and y.

The STD and RMSE data mentioned is computed for each possible position of the emitter in the lattice and is then plotted, as it is shown in **Figure 2.4.**

In **Figure 2.4.** the existence of a convergence region aforementioned in **Figure 2.3.** is shown clearer, especially in **Figure 2.4.C.**

Furthermore, the CRB is determined with the following equation, derived from **equation 1.10.:**

$$\tilde{\sigma}_{CRB}(\vec{r}) = \frac{L}{2\sqrt{2N}} \left(1 - \frac{L^2 \ln(2)}{fwhm^2}\right)^{-1} \sqrt{\left(1 + \frac{1}{SBR(\vec{r})}\right) \left(1 + \frac{3}{4 SBR(\vec{r})}\right)}, \quad (2.6.)$$

where SBR is the signal-to-background ratio:

$$SBR(\vec{r}) = \frac{\sum_{i=0}^{K-1} \lambda_i}{4\lambda_b} \approx \frac{c_{eqe\sigma a} \sum_{i=0}^{K-1} I_i(\vec{r})}{4\lambda_b}, \quad (2.7.)$$

see **equation 1.3.** for the symbols. Calculating the CRB for each possible position of an emitter in the sample, the mean value of the CRB obtained is 1.22 nm.

The execution time of this code is of 3 hours in a computer with Intel7-6700HQ, 16 GB of RAM and a GPU NVIDIA GTX960M.

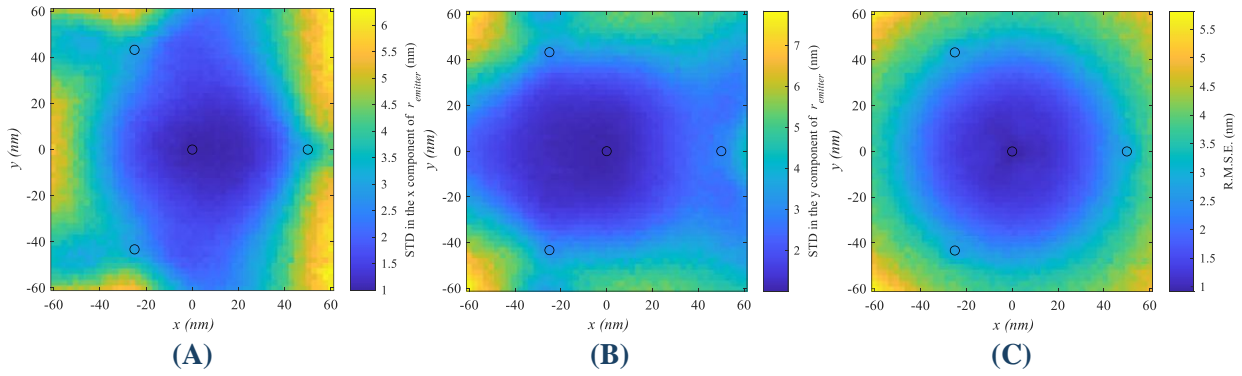


Figure 2.4. (A) Standard Deviation for the x component of $\vec{r}_{emitter}$, in nm. (B) Standard Deviation for the y component of $\vec{r}_{emitter}$, in nm. (C) Root Mean Squared Error for the estimation of the emitter's location, in nm. Simulation done for $L = 100$ nm, $N = 1000$ and $fwhm = 360$ nm. It can be seen that, as assumed, the circumference that the vertices of the equilateral triangle corresponding to the different beam positions comprises the convergence region.

2.2. Examining the potential of the method

Once the main setup is established, for a better understanding of the method, to research if it is possible to improve its performance, and in order to define the need of changing the created code when the conditions differ, several tests are to be done. With different shapes for the illumination beam, a different setup and trying to reduce manually the area of the beam, to avoid overlapping.

2.2.1. Rhombic pattern

In [11] it has been proven that with a donut-shaped beam, illuminating four times the sample with beam positions forming an equilateral triangle and its centroid, has a better performance than only doing one measurement also with the donut-shaped beam or with flat-field illumination.

To confirm this statement, one possible approach is to look at the likelihood function for four different situations. In each of them, a different number of illuminating beam

positions, from one to four progressively, and with different locations, is used to activate the molecules in the sample, as in **Figure 2.5.**, where the emitter is situated at (11,6) nm.

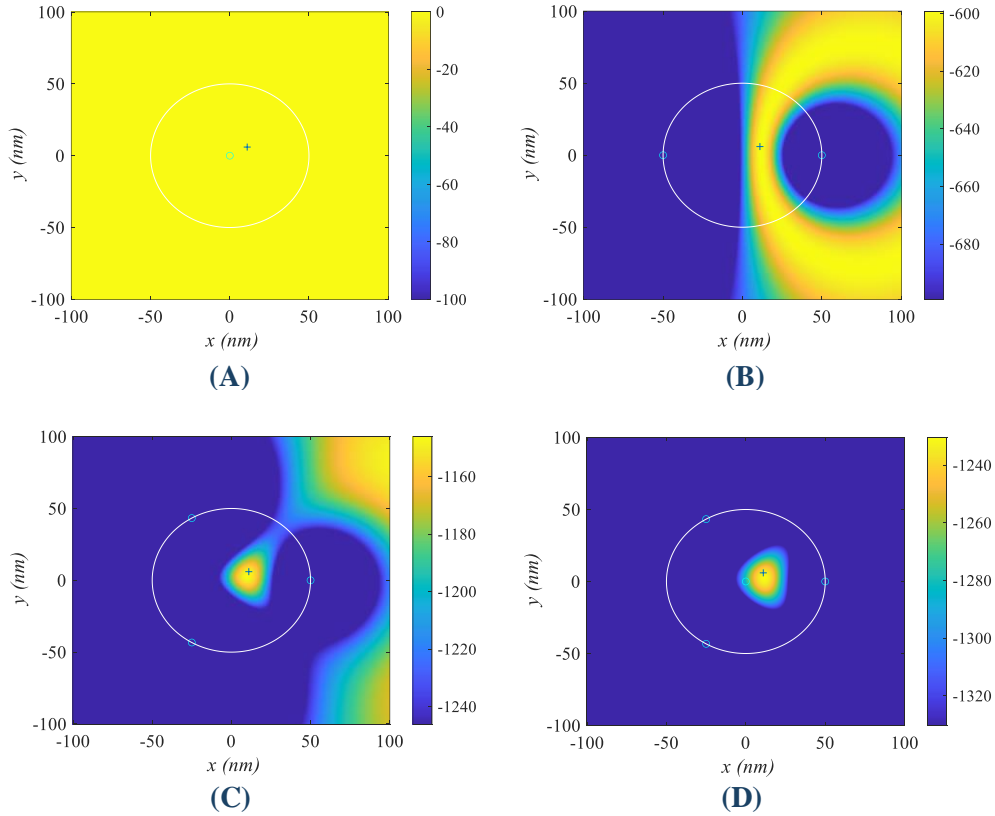


Figure 2.5. (A) Likelihood function for a simulation done with one beam. (B) Likelihood function for a simulation done with two beams. (C) Likelihood function for a simulation done with three beams. (D) Likelihood function for a simulation done with four beams, as in MINFLUX. Each experiment done for $L = 100$ nm, $N = 1000$ and $fwhm = 360$ nm, for an emitter located at $x = 11$ nm and $y = 6$ nm.

It can be seen that it is not possible to determine the position of the fluorophore with just one illumination donut-shaped beam because the likelihood function has the same value for every position of the lattice, zero. Nonetheless, when the number of exposures of the sample is increased, it is shown that it gets increasingly more plausible to locate the emitter, as the region where the likelihood function has a greater value diminishes gradually. However, the estimation presents a high error until four beams are used.

Despite that, there is no explicit reason to explain the decision of using the “*equilateral triangle and centroid*” pattern to illuminate the sample. Therefore, one can try another setup for the beam positions with the aim of improving the efficiency of the method.

In this work, it has been followed the hypothesis that a parallelogram-based beam distribution in space, if the shape has good symmetry properties, would have a nice performance such as the equilateral triangle. As a rhombus is like mirroring the equilateral triangle, the distribution of the beams to try will follow that shape. The new configuration

will follow the same pattern as in [section 2.1](#). changing the centroid position to that of the rhombus and positioning a fifth beam as the fourth vertex of the rhombus.

Besides, from the known information on the likelihood function thanks to the previous analysis, one might expect that adding a new beam position will make the estimate better.

A modification to the MATLAB code generated in [section 2.1](#). has been done in order to simulate the situation stated in this section and conclude whether or not the new pattern of exposures of the sample is more efficient and gives better localization precisions. The new code can be found in the [Annex](#) of this thesis.

From [Figure 2.6](#). one can conclude that the original beam distribution showed a greater performance, because although the symmetries of STD and RMSE are respectively very similar to those in [Figure 2.4.](#), the value of the error increases, especially outside the convergence region.

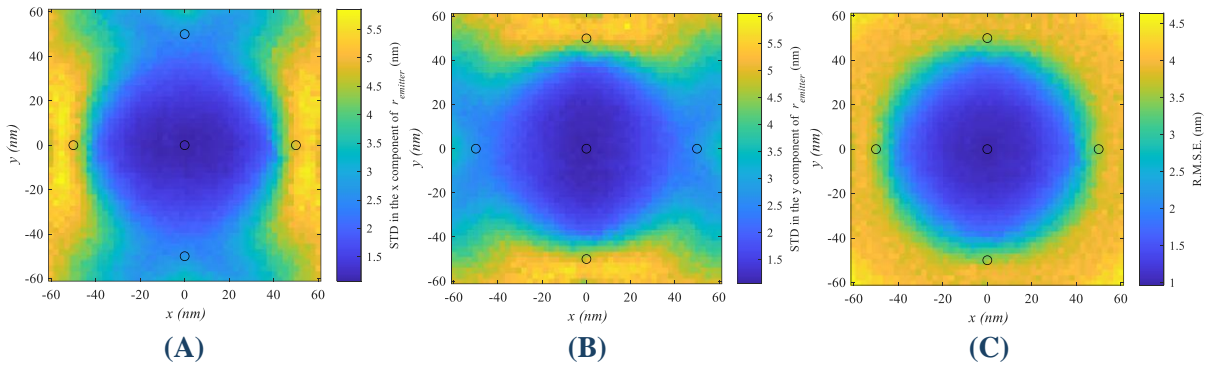


Figure 2.6. (A) Standard Deviation for the x component of $\vec{r}_{emitter}$, in nm. (B) Standard Deviation for the y component of $\vec{r}_{emitter}$, in nm. (C) Root Mean Squared Error for the estimation of the emitter's location, in nm. Simulation done for $L = 100$ nm, $N = 1000$ and $fwhm = 360$ nm.

Moreover, if the emitter position coincides with some of the beam, the estimation would be less precise for the rhombus setup case than for the original, which shows a subtle decrease in error in this specific situation that can be seen in [Figure 2.4.C](#).

In spite of that, the fact that the alleged hypothesis in this section was false does not imply that there is no other setup that provides a better performance, but that it is not intuitive. Perhaps one could find a better beam distribution with a Deep Learning algorithm, although it is not one of the objectives of this thesis.

2.2.2. Parameters study

To determine if the MINFLUX parameters (L , N and $fwhm$) have a direct influence in the efficiency of the method and what effect changing their value has, a parameter study will be performed, creating a MATLAB code that can be found in the [Annex](#).

In order to analyse the data with objective judgement the STD of the emitter position estimations will be calculated for a fixed fluorophore located at (11,6) nm, under a set of

different conditions. The settled values of the parameters have been chosen among others for convenience.

◆ Fixed $fwhm = 360$ nm and $N = 1000$, and varying L :

It is known in advance that reducing L below 10–20 nm is not very consistent since the region through which the beams are moved must contain the emitter, which may be of some nanometres in size. In **Figure 2.7**, that can be ascertained, because below approximately $L = 10$ nm, the Standard Deviation values for x and y start to increase.

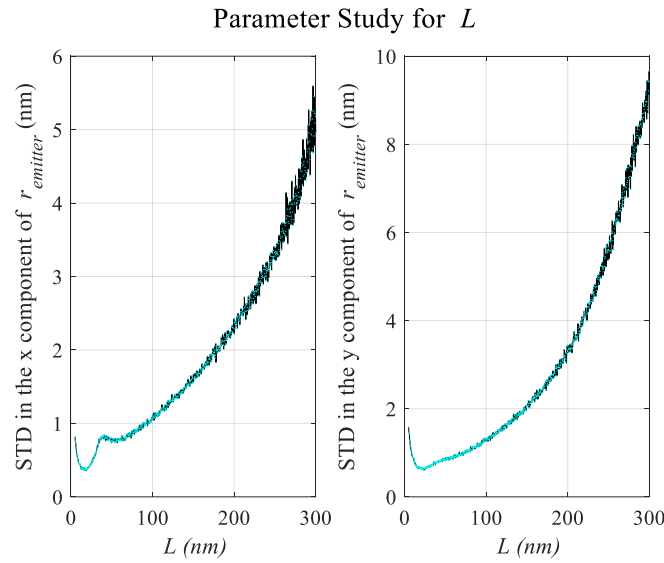


Figure 2.7. STD dependence on L , for an emitter situated at $x = 11$ nm and $y = 6$ nm, with $N = 1000$ and $fwhm = 360$ nm.

There is no reason to justify the small increase of standard deviation that can be seen just before $L = 50$ nm in the figure for the STD in the x component of $r_{emitter}$, other than that the standard deviation may also be affected by the behaviour of N or $fwhm$ for that fixed L . Therefore, the same analysis will be done for $L = 50$ nm, to study that phenomena.

In the simulations done in this project, $L = 100$ nm is the standard value used. The STD obtained with it is within the range of the acceptable and with that L fixed, N and $fwhm$ also show a good STD.

◆ Fixed $L = 100$ nm and $fwhm = 360$ nm, and varying N :

In **Figure 2.8**, one can see the dependence of the STD on N . It is noticeable that by increasing the number of photons emitted one obtains a better localization.

However, this result is not surprising, but one should remind that in MINFLUX the principal aim is to reduce the value of N . Thus, what one should try in order to obtain a good estimation of the emitter's position is to have the lowest STD possible.

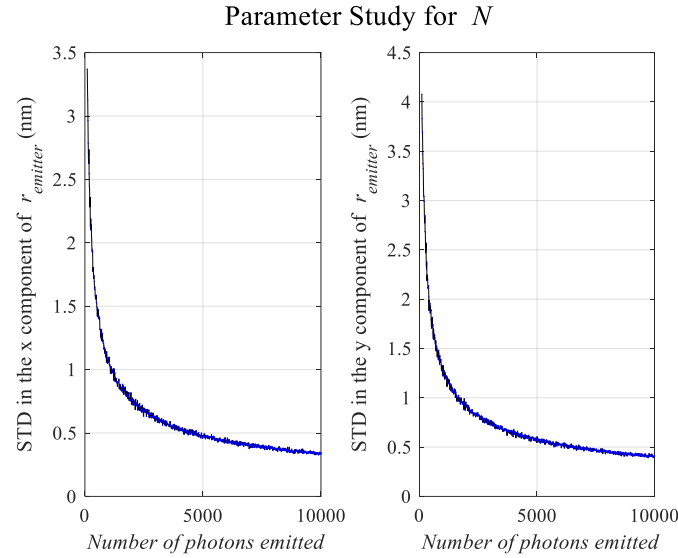


Figure 2.8. STD dependence on N , for an emitter situated at $x = 11$ nm and $y = 6$ nm, with $L = 100$ nm and $fwhm = 360$ nm.

Between 1 and 1.5 nm of STD is a range of error acceptable and which can be assumed to have the benefit of being in a low N -range of between 100 and 1000, which are the main values used in this thesis.

◆ Fixed $L = 100$ nm and $N = 1000$, and varying $fwhm$:

The size related parameter $fwhm$ is limited by two things. On one hand, the diffraction limit is a lower bound to its value. The system that is simulated has a $NA = 1.45$ and $\lambda = 580$ nm, then the diffraction limit is of 200 nm. On the other hand, if one wants to avoid overlapping the beam cannot have a very large area.

As seen in **Figure 2.9.**, for high values of $fwhm$, approx. from 500 nm, the STD starts to increase, as expected. From the results in the plot, one can conclude that the perfect range of $fwhm$ is between 200 and 400 nm for the STD in the x component and from 400 to 600 nm for the STD in the y component. Accordingly, the interval of values that will probably give the best results will be between 300 and 500 nm. In this thesis $fwhm$ is set to 360 nm, as it is also done for some simulations in [11].

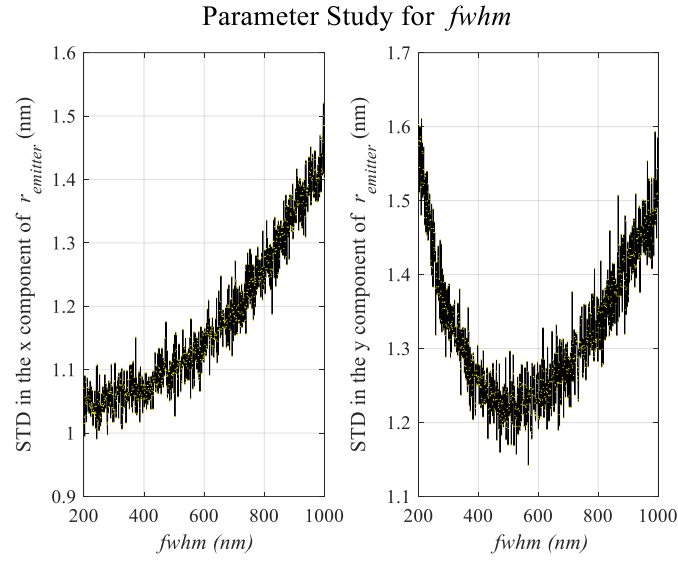


Figure 2.9. STD dependence on $fwhm$, for an emitter situated at $x = 11$ nm and $y = 6$ nm, with $N = 1000$ and $L = 100$ nm.

- ◆ Fixed $L = 50$ nm and $fwhm = 360$ nm, and varying N :

Figure 2.10. shows the dependence of the STD on N for an L value of 50 nm. In this case, in contrast to L being set to 100 nm, the STD is slightly smaller, giving values below 1 nm for $N = 1000$, which is a good improvement. However, no other significant change is observed.

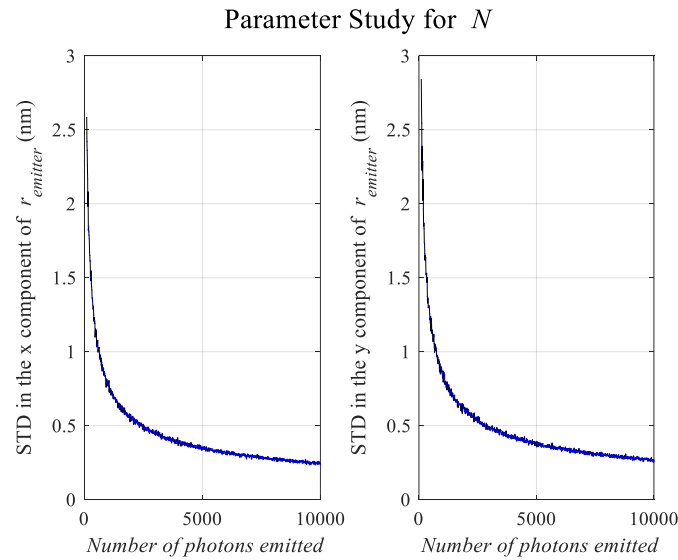


Figure 2.10. STD dependence on N , for an emitter situated at $x = 11$ nm and $y = 6$ nm, with $L = 50$ nm and $fwhm = 360$ nm.

Therefore, there is no explanation in the $fwhm$ values for the increase of the STD for L near 50 nm.

- ◆ Fixed $L = 50$ nm and $N = 1000$, and varying $fwhm$:

In **Figure 2.11**, one can see the dependence of the STD on $fwhm$. In this case it is noticeable that the STD is lower than when $L = 100$ nm, for a wider range of $fwhm$ values. Furthermore, it can be appreciated in the figure that the comparatively high STD values in the "y" component that could be observed for $fwhm$ of about 200 nm in the case with $L = 100$ nm have disappeared, decreasing to almost half. When $L = 50$ nm, consequently, it is possible to limit the $fwhm$ to a range of between 200 and 400 nm, which would mean a less wide scan region in addition to a smaller PSF footprint.

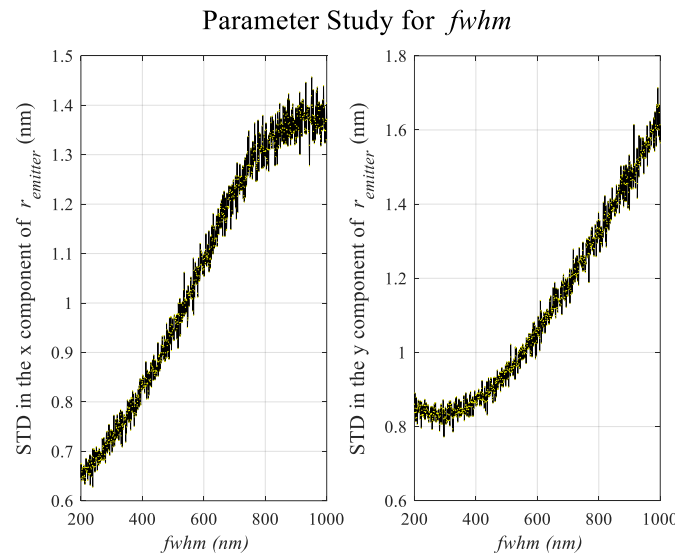


Figure 2.11. STD dependence on $fwhm$, for an emitter situated at $x = 11$ nm and $y = 6$ nm, with $N = 1000$ and $L = 50$ nm.

In this case, similar results to the previous analysis are obtained, in which no correlation can be identified to explain the rise of the STD in L s close to 50 nm. Hence, further study is needed to reach a conclusion. Since all simulations will be made for $L = 100$ nm for the reasons already mentioned, this discussion will be postponed to be made in case there is enough time.

According to these results, one could be tempted to do the simulations with a scanning region $L = 50$ nm instead of 100 nm, but this is not ideal because firstly one should approximate the position of the molecule, which size will be of some nanometres [14], to set the FOV of the SMLM experiment, and that is easier with a higher L .

2.2.3. Shrinkage of the PSF area

One of the objectives of this thesis is to reduce the area of the PSF of the imaging system. Thus, overlapping between PSFs would be dwindled or even eliminated, which would allow for a more precise localization. In this section, the hypothesis is that giving a lower value to the size-parameter $fwhm$ of the donut-shaped beam, e.g. 260 nm, the overlapping probability will decrease while maintaining or even improving the efficiency of the method.

The comparison between the shape of the beam with the established $fwhm$ and when $fwhm = 260$ nm can be seen in **Figure 2.12**.

To check whether the hypothesis is fulfilled or not, one must look at **Figure 2.13**. As it can be observed, although the convergence region that was obtained with the original setup and that can be seen in **Figure 2.4** is maintained, the STD and RMSE values have risen, with a considerable increase in the situations where the emitter location coincides or is near the position of the beams. Hence, one can conclude that the $fwhm$ parameter is not the only parameter to be adjusted to shrinkage the PSF area.

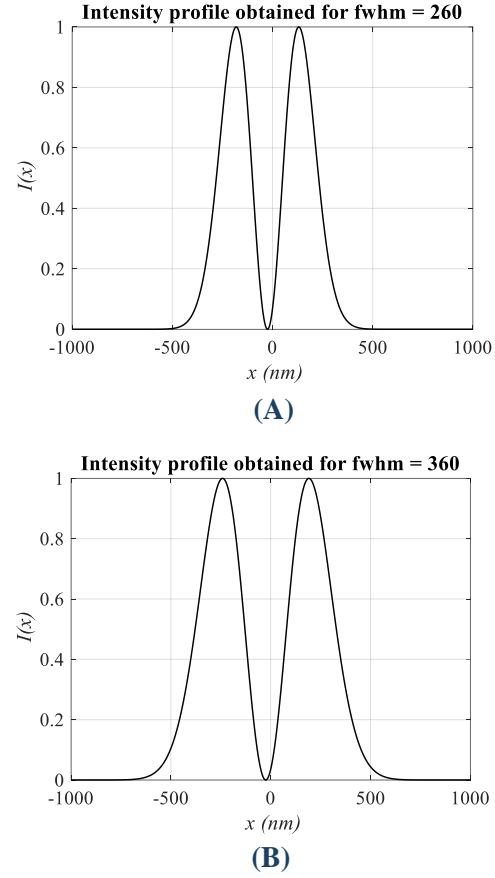


Figure 2.12. Transversal cut of the donut-shaped PSF intensity profile for $L = 100$ nm, $N = 1000$ and (A) $fwhm = 260$ nm or (B) $fwhm = 360$ nm.

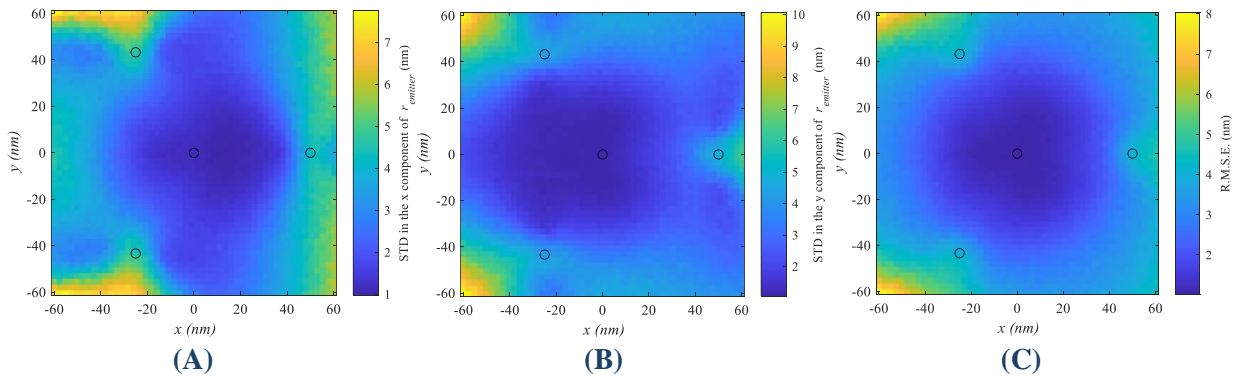


Figure 2.13. (A) Standard Deviation for the x component of $\bar{r}_{emitter}$, in nm. (B) Standard Deviation for the y component of $\bar{r}_{emitter}$, in nm. (C) Root Mean Squared Error for the estimation of the emitter's location, in nm. Simulation done for $L = 100$ nm, $N = 1000$ and $fwhm = 260$ nm.

2.2.4. Illumination beam: Parabolic shape

When the Deep Learning is performed and the learned mask generated, one will have a beam with another shape rather than a toroid. To know how the method will behave illuminating with a differently shaped beam, a parabola-shaped beam will be used to repeat the simulation. This shape is chosen among others because it is the best approximation to the donut shape although being physically impossible to realize, and also the direct computation of some needed formulas is described in [11]. The intensity of the PSF in this situation follows:

$$I_{parabola} = A_0 r^2, \quad (2.8.)$$

with r as stated in [equation 2.2.](#), and A_0 a normalization constant. As the minimum of the donut resembles a parabola, similar behaviour is expected from the simulation in both cases.

The MATLAB code generated in [section 2.1.](#) has been modified to simulate the situation stated in this section and conclude whether or not the new shape of the beam gives better localization precisions and a wider convergence region. This can be found in the [Annex](#) of this thesis.

As one can see in [Figure 2.14.](#), using a parabola-shaped beam with the same parameters as in [section 2.1.](#) results in the deformation of the convergence area and the worsening in the location of emitter positions near or coincidental to the beam ones, although obtaining in general lower RMSE and STD values.

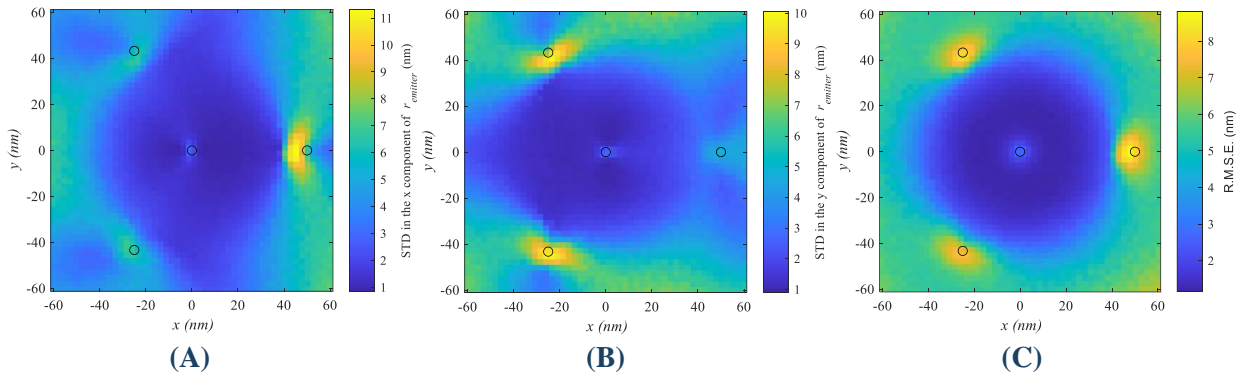


Figure 2.14. (A) Standard Deviation for the x component of $\bar{r}_{emitter}$, in nm. (B) Standard Deviation for the y component of $\bar{r}_{emitter}$, in nm. (C) Root Mean Squared Error for the estimation of the emitter's location, in nm. Simulation done for a parabola-shaped beam with $L = 100$ nm, $N = 1000$ and $fwhm = 360$ nm.

Nonetheless, as the beams used are different, one reason this configuration behaves worse could be that some parameters have to be readjusted. Thus, the simulation will be done again changing the total number of photons (N) to $N = 100$, but maintaining L and $fwhm$. The interest of the method still lies in having the less PSF footprint possible, therefore

increasing L or $fwhm$ would have no benefit, and those parameters have limits on how low they can be, as seen in previous sections.

Using this new parameter configuration, the convergence region recovers the symmetry although shrinking, and the recovering of emitter positions with the MLE when the fluorophore is near or coincides with the position of the beam is done with a substantially smaller error than in the previous case, results that are shown in **Figure 2.15**.

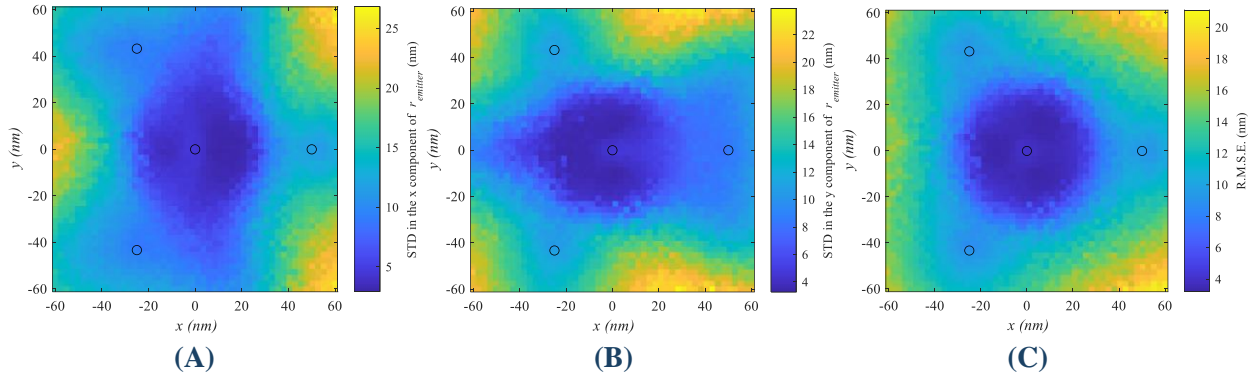


Figure 2.15. (A) Standard Deviation for the x component of $\bar{r}_{emitter}$, in nm. (B) Standard Deviation for the y component of $\bar{r}_{emitter}$, in nm. (C) Root Mean Squared Error for the estimation of the emitter's location, in nm. Simulation done for a parabola-shaped beam with $L = 100$ nm, $N = 100$ and $fwhm = 360$ nm.

However, comparing the convergence region and the error with the original case showed in **Figure 2.4**, may be inaccurate as the parameters of each simulation are different. Therefore, the experiment done in **section 2.1**, will be repeated but with $N = 100$ to be able to compare both cases properly. The results of this analysis can be seen in **Figure 2.16**. One may be surprised by the similarity between outcomes.

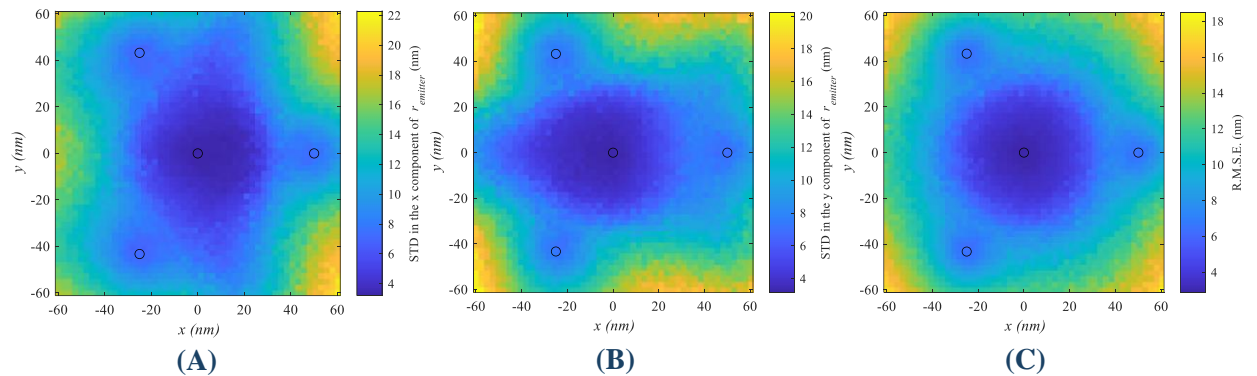


Figure 2.16. (A) Standard Deviation for the x component of $\bar{r}_{emitter}$, in nm. (B) Standard Deviation for the y component of $\bar{r}_{emitter}$, in nm. (C) Root Mean Squared Error for the estimation of the emitter's location, in nm. Simulation done for a donut-shaped beam with $L = 100$ nm, $N = 100$ and $fwhm = 360$ nm.

The conclusions that one could draw from comparing **Figure 2.15**, and **Figure 2.16**, are that it seems that when a parabolic shaped beam is used, one can see a greater precision

in the location of emitters that are outside the convergence region, while in the case of the donut-shaped beam a better performance within this region and when the position of the active molecules coincides with those of the beam is obtained.

In MINFLUX, the interest lies in having an emitter as close to the illumination beam's position as possible, such that the photon budget is the lowest. For that reason, the donut-shaped beam would still be the best choice for the method even if the quadratic beam was possible to generate. Besides, it is interesting to compare the STD and RMSE matrixes obtained for each different shaped beam with themselves for a different N.

The difference for the case of the donut-shaped beam is not substantial, it is observed that for N = 100 the area of convergence is reduced while the error increases with respect to the same procedure for N = 1000. In contrast, with regard to the parabolic beam, a much more significant discrepancy can be observed, with a very considerable decrease in the error for N = 100 in the emitter positions coinciding with those of the beam, and a greater uniformity in the area of convergence but with more error than for N = 1000.

2.2.5. Illumination beam: Gaussian shape

Another shape of the beam that one could try for this experiment is the Gaussian beam, because if the MINFLUX technique could be done with it, a more basic and simpler setup could be used for a SMLM experiment, e.g. a Confocal Microscope. Notwithstanding this, one could expect this simulation to fail in performing the method properly, as the Gaussian beam has no minima but a maximum, as it can be seen when plotting the intensity profile for the PSF of a Gaussian beam:

$$I_{Gauss} = A_0 e^{-4 \ln 2 \frac{r^2}{fwhm^2}}, \quad (2.9.)$$

with r as stated in [equation 2.2.](#), and A_0 a normalisation constant.

The MATLAB code generated in [section 2.1.](#) has been modified to simulate the situation stated in this section and conclude whether or not the new shape of the beam gives better localization precisions and a wider convergence region. This can be found in the [Annex](#) of this thesis.

In [Figure 2.17.](#) and [Figure 2.18.](#) one can see that the results agree with the prediction, and that changing the value of the parameter N makes no difference in convergence in this case.

However, it could be possible to perform the method only using the slope of the Gaussian beam, and therefore having a suitable option for MINFLUX because there would be no maxima, a suitable minimum and the expected gradient of illumination intensity.

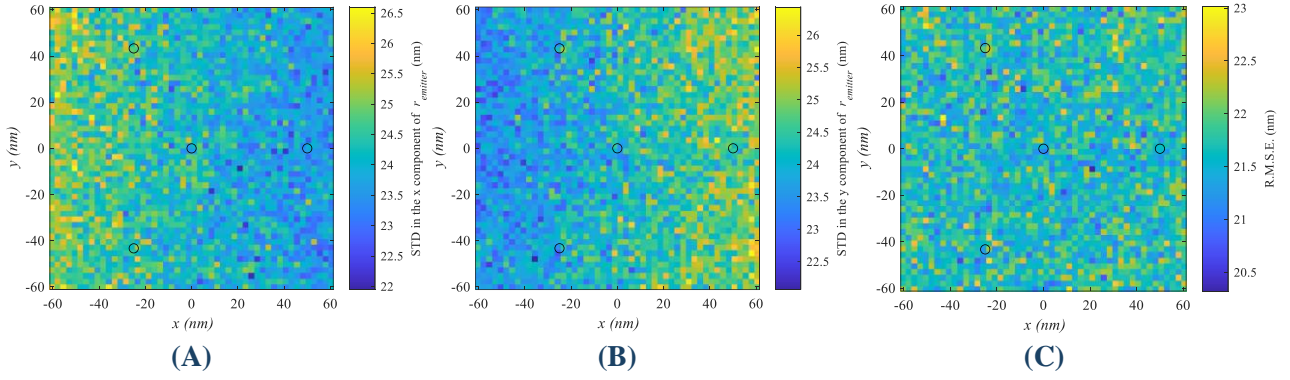


Figure 2.17. (A) Standard Deviation for the x component of $\bar{r}_{emitter}$, in nm. (B) Standard Deviation for the y component of $\bar{r}_{emitter}$, in nm. (C) Root Mean Squared Error for the estimation of the emitter's location, in nm. Simulation done for a Gaussian beam with $L = 100$ nm, $N = 1000$ and $fwhm = 360$ nm.

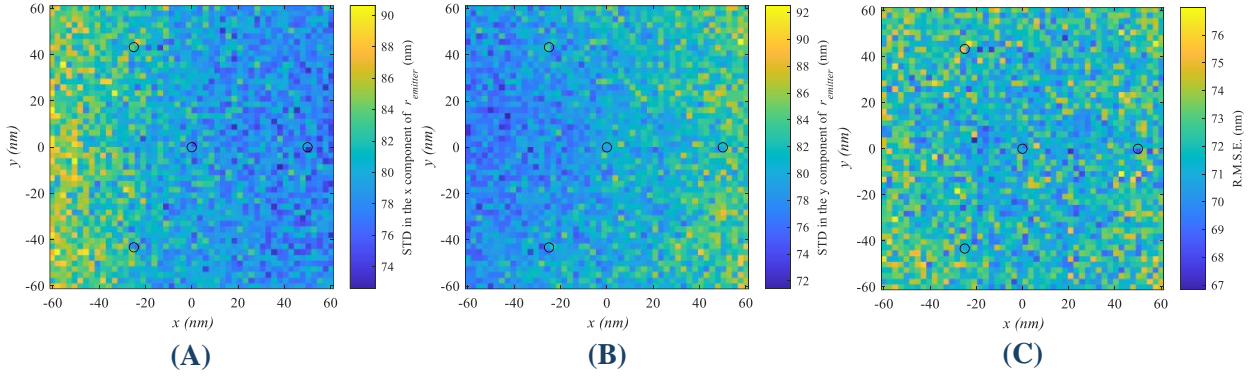


Figure 2.18. (A) Standard Deviation for the x component of $\bar{r}_{emitter}$, in nm. (B) Standard Deviation for the y component of $\bar{r}_{emitter}$, in nm. (C) Root Mean Squared Error for the estimation of the emitter's location, in nm. Simulation done for a Gaussian beam with $L = 100$ nm, $N = 100$ and $fwhm = 360$ nm.

This will be implemented such that the intensity profile of the PSF for this situation, which is shown in **Figure 2.19.**, follows:

$$I_{Gslope} = A_0 h(r - 100) e^{-4 \ln 2 \frac{r^2}{fwhm^2}} h(510 - r), \quad (2.10.)$$

with r as stated in **equation 2.2.**, h the Heaviside function and A_0 a normalisation constant.

The MATLAB code is now modified to simulate this situation and determine whether or not the slope of the Gaussian beam is a good alternative in MINFLUX, giving better localization precisions and a wider convergence region while allowing the use of a Confocal Microscope. This new code can be found in the Annex of this thesis.

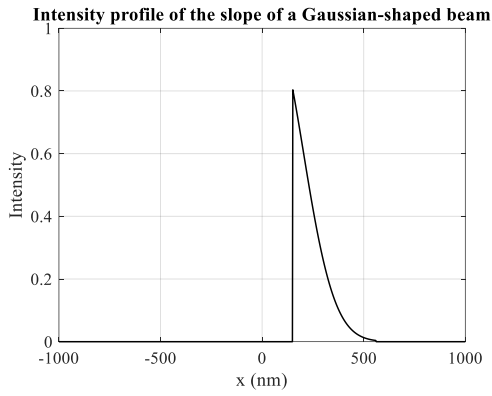


Figure 2.19. Transversal cut of the slope of the Gaussian-shaped PSF intensity profile for $L = 100$ nm, $N = 1000$ and $fwhm = 360$ nm.

Then, after some days of execution the results that can be seen in **Figure 2.20**, are obtained. Lower values of STD and RMSE are achieved, but higher than those from previous analysis. Furthermore, it is difficult to determine if the STD and RMSE matrices that are depicted in **Figure 2.20**, are correct, since the resulting images look like the PSF of the system, which is unusual, and an aberrant result may have been obtained. However, this distribution of error would also imply that the slope is not a good alternative to the Gaussian beam, because it is still not possible to accurately localize and emitter. Hence, it has been impossible to

properly apply the MINFLUX method with a Gaussian beam.

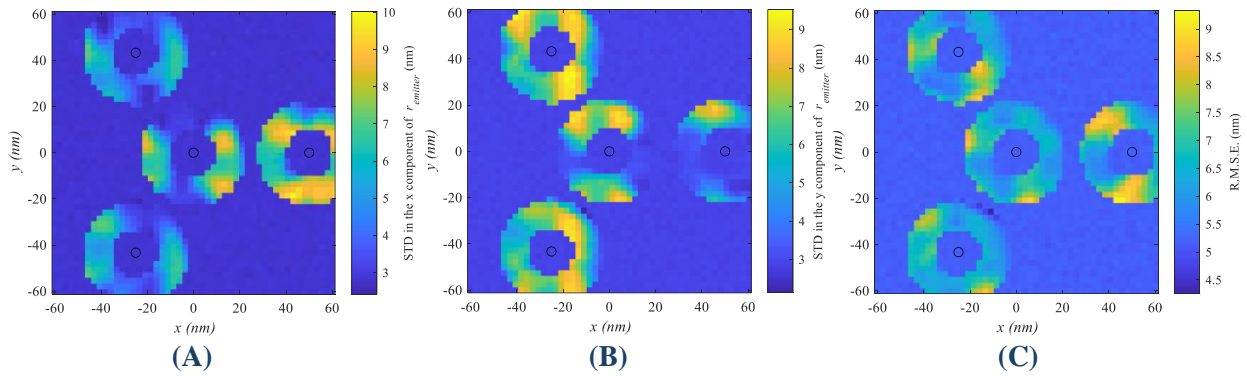


Figure 2.20. (A) Standard Deviation for the x component of $\vec{r}_{emitter}$, in nm. (B) Standard Deviation for the y component of $\vec{r}_{emitter}$, in nm. (C) Root Mean Squared Error for the estimation of the emitter's location, in nm. Simulation done for $L = 100$ nm, $N = 100$ and $fwhm = 360$ nm.

2.3. Deep Learning – Functions for MINFLUX

With the purpose of analysing if the PSF shape obtained after completing the Deep Learning has a better performance than the donut-shaped, a MATLAB code that can be found in the Annex of this thesis is created to compute the CRLB from the Fisher Information Matrix of the model, as seen in **section 1.3**. Notice that this implies that once one has the results of the Deep Learning algorithm, it would be necessary to describe an analytical model for the PSF to be able to evaluate its efficiency in MINFLUX. The CRLB is calculated for a specific position of an emitter and a range of total number of photons, as a result of the conclusions of previous simulations. If used with the already introduced MINFLUX method, one obtains the results depicted in **Figure 2.21**.

This code could also be modified into a function to obtain the CRLB for every possible position of the fluorophore in the lattice simulated in the original experiment, as done to compute the STD and RMSE of the method.

On the other hand, in the loss function of the Deep Learning code, another variable that is interesting to introduce is the Area of the PSF, which would be ideal to reduce as much as possible without compromising resolution. Thus, a code computing the length in x and y of the footprint of the PSF is generated, and can also be found in the Annex. It has been programmed in MATLAB but to be adapted to the Deep Learning code, it will be rewritten in Python and inserted as required.

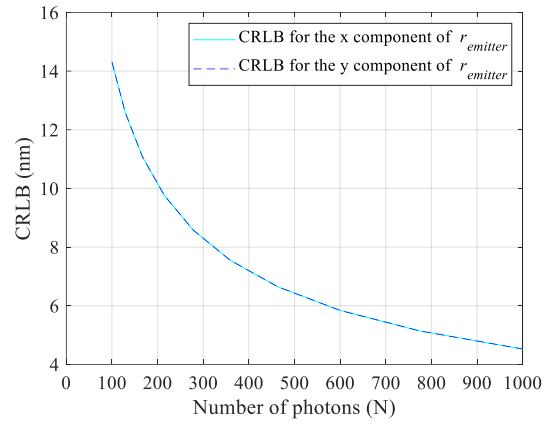


Figure 2.21. CRLB in the x and y direction for an emitter located at (50,50) nm with $L = 100$ nm, $fwhm = 360$ nm and varying N from 100 to 1000 photons.

2.4. Deep Learning – Learned Mask

When imaging a cell or an organism with a microscope, usually flat illumination is used. Nevertheless, it could be interesting to change the pattern of the incident light, as in the case explored in this project. This can be done introducing a Spatial Light Modulator (SLM) to the imaging path of the microscope, in the back focal plane or pupil plane, as shown in the schematic presented in **Figure 2.22**.

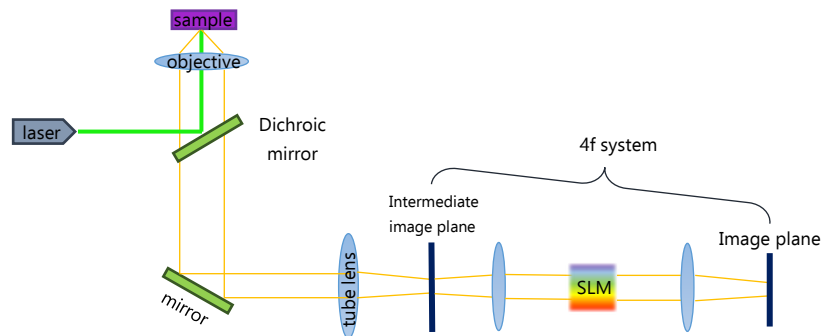
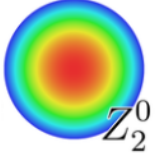

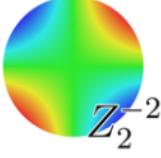

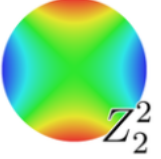

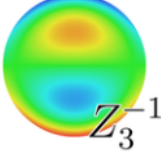

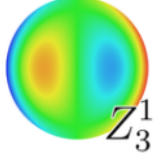

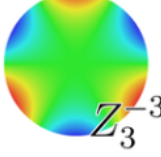

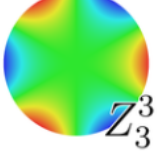
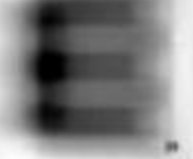


Figure 2.22. Scheme of a fluorescence microscope for SMLM with a Spatial Light Modulator as in DeepSTORM.

The SLM can be used to modulate the phase of the beam, i.e. it introduces a phase mask that changes the PSF of the system. It can be placed either in the illumination path to adjust its shape or in the imaging path as in **Figure 2.22**. to improve the final resolution. Phase masks are optical elements that generate interferences within the beam's light in order to enhance contrast or improve image resolution. These masks modify what is called the Pupil function, that describes how a light wave is affected upon transmission through an optical imaging system, i.e. indicates the change in amplitude and phase of the wave.

A phase mask is usually produced with the combination of one or more Zernike Polynomials to parametrise the phase, and is commonly used to correct or create aberrations. In **Table 2.1.** there is a brief description of how this works for the most frequent ones [7], [8], [15]–[17].

Table 2.1. Most common Zernike coefficients and polynomials, and the aberrations that they can correct or produce. Images obtained from [18], [19].

Zernike Coefficient	Zernike Polynomial	Name (Aberration to correct)	Image of the phase mask	Image of the aberration
Z_4	$\sqrt{3}(2\rho^2 - 1)$	Defocus	 Z_2^0	
Z_5	$\sqrt{6}\rho^2 \sin(2\theta)$	Astigmatism 45° (oblique)	 Z_2^{-2}	
Z_6	$\sqrt{6}\rho^2 \cos(2\theta)$	Astigmatism 0° (vertical)	 Z_2^2	
Z_7	$\sqrt{8}(3\rho^3 - 2\rho) \sin(\theta)$	Vertical coma	 Z_3^{-1}	
Z_8	$\sqrt{8}(3\rho^3 - 2\rho) \cos(\theta)$	Horizontal coma	 Z_3^1	
Z_9	$\sqrt{8}\rho^3 \sin(3\theta)$	Field curvature 30°	 Z_3^{-3}	
Z_{10}	$\sqrt{8}\rho^3 \cos(3\theta)$	Field curvature 0°	 Z_3^3	

In DeepSTORM3D [12] the mask is used to modify the PSF in the imaging path to avoid overlapping of PSFs in the image of the sample. This phase mask is generated using a Deep Learning algorithm, which trains a Convolutional Neural Network (CNN) that allows the learning of a mask optimised for 3D localization of emitters.

A CNN is an algorithm of Deep Learning that is used to analyse and classify images, differentiating the components of the picture. To do the latter, some parameters or characteristics of the image are assigned as weights, that are to be learned in order to be optimised. In this case, the parameters describing the phase mask are an example of weights. The typical input image to a CNN is read as a 3D matrix, a box containing the dimensions of height and width in pixels of the picture but also three layers, known as channels, corresponding to the digital colours RGB (Red–Blue–Green) encoding. Notwithstanding that, the input image can also be in a grey chromatic scale.

A CNN learns from an image carrying out the convolution operation applying filters, also known as Kernels. The network can be programmed with more than one Convolutional Layer, adding layers according to the specificness of details that need to be detected from the image. The CNN has the role to reduce the images into an easier-to-process form, without losing features that are crucial to obtain a good prediction [20]–[22].

The CNN of the original code used in this thesis has ten Convolutional Layers. The whole algorithm is programmed using Pytorch, a Python tool for Deep Learning, and it can be found in [23]. The main code is `demo4.py` and, to work, it needs some functions that are also defined in the GitHub folder, like `parameter_setting_demo4.py`, `helper_utils.py`, `loss_utils.py`, `cnn_utils.py`, `physics_utils.py`, `data_utils.py`, `vis_utils.py`, `GenerateTrainingExamples.py` and `PSF_learning.py`. The running time of the whole experiment is of 63 hours in a server with 80 cores, a CPU 2x Intel Gold 6148, 384 GB of memory and a GPU 4x Tesla P100.

The code generates its own training images that are also used for learning, and trains the network to be able to precisely localize molecules in an image taken in a SMLM experiment with a CCD camera, obtaining at the same time a learned phase mask that is used to generate a PSF which is supposed to avoid overlapping between emitters' PSFs in 3D. A flowchart describing its operation mode can be seen in **Figure 2.23**.

In this project, the aforementioned algorithm will be changed as explained in the following subsections in order to obtain a phase mask optimised for 2D localization using the MINFLUX conditions. The aim of this procedure is to have a PSF that presents a minimum to reduce the photon budget, the footprint of which is as small as possible and which shape is adapted to avoid overlapping between emitters' PSFs. The phase mask designed should be placed in the illumination path of the microscope to change its PSF, instead of in the imaging path as in DeepSTORM3D.

All corrections done to the code can be found in the **Annex** of this thesis. However, in the following subsections the most relevant ones are to be explained.

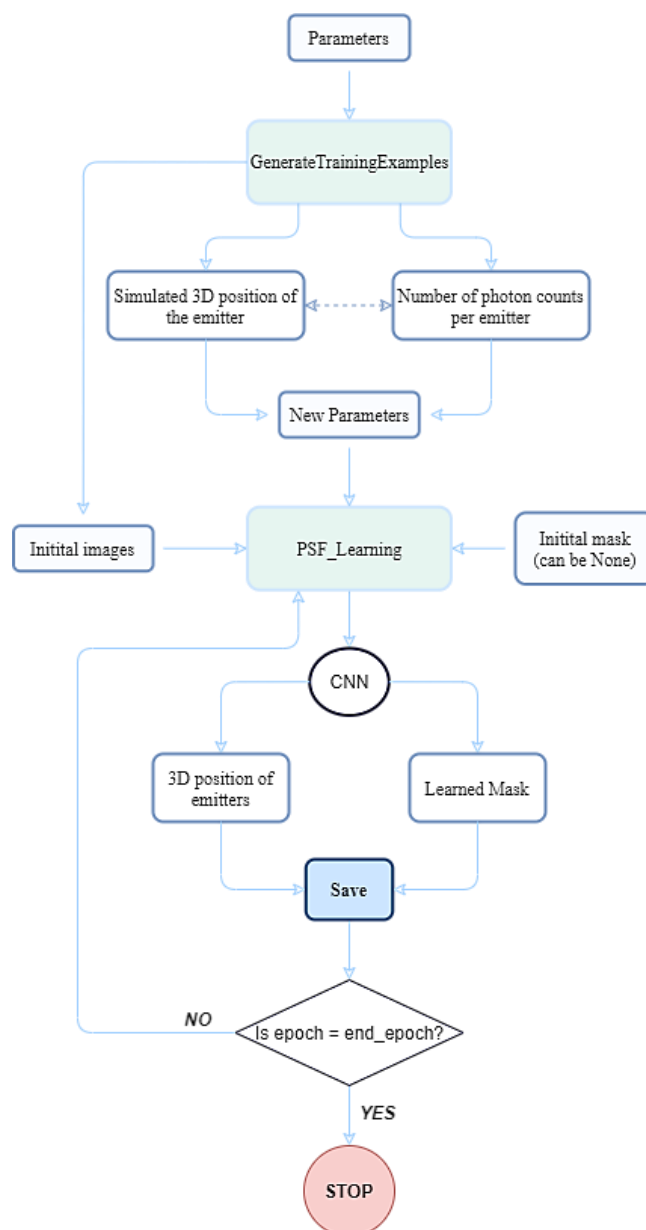


Figure 2.23. Flowchart describing the code [23] to localize emitters in a sample and learn a phase mask that changes the shape of the 3D PSF of the system to avoid overlapping.

2.4.1. Changes in parameter_setting_demo4.py

It is necessary to change the phase mask and image space dimensions for simulation parameters in order to agree with our number of dimensions. The z-range and discretization in the axial direction have to be removed. The number of particles' range will also be modified, fixing a total of 5 fluorophores per sample, to reduce the execution time of the code and to ease it.

A special section to set the parameters that are needed for MINFLUX is to be introduced, defining the Poisson noise (λ_b) of the measurement, c_e , q_e , σ_a , the diameter of the circumference formed by the beam positions (L) and the size parameter $fwhm$.

2.4.2. Changes in data_utils.py

The grid positions of the emitters in the sample have to be adapted to the new two-dimensional space. Moreover, the function to generate a Boolean grid from the positions of the fluorescent molecules can be removed, as images will no longer be used when the adaptation to MINFLUX is done.

In this code a uniform distribution for the total number of photons (N) is applied, meaning that each emitter is assigned a value between 1000 and 6000 of total photons emitted.

2.4.3. Changes in physics_utils.py

To be able to locate the fluorophores two-dimensionally instead of in 3D, the axial dimension will be removed from all subfunctions and parameters.

Furthermore, the computation of the number of photon counts (n_i) per molecule stipulated in MINFLUX has to be introduced in a new Physical Layer. For every emitter, with its own total number of photons determined in data_utils.py, one should have four photon counts corresponding to the different intensities detected when measuring with the four different beam's positions. Thus, it is also necessary to introduce the calculus of those intensities.

In this code, there is a function that calculates the phases in the Fourier space for the given emitter positions. This is necessary to obtain the phase mask. Changing the three-dimensionality in this algorithm will imply a learned mask that produces a two-dimensional PSF.

If one were to place the SLM in the imaging path as in DeepSTORM, the image that would correspond to every switch would have to be simulated, obtaining the PSF of the system for every exposure of the sample and summing them to have the intensity function of the imaging path, the convolution of which with the phases in the Fourier space for the given emitter positions would lead to the final image of the sample.

This was the procedure taken initially but after reviewing all the changes it was seen that a whole new environment should be introduced to situate the SLM in the illumination path, as MINFLUX would require, instead.

2.4.4. Changes in loss_utils.py

The loss function has a key role in a Deep Learning algorithm because it is determinant to define whether it is working properly or not, i.e. a progressive decrease of the loss will mean a gradual achievement of the objectives of the network. In the situation described in this project, the less the loss, the more accurate the localization of the emitters.

The loss function of DeepSTORM3D uses a Kernel Density Estimation (KDE), with a Gaussian-shaped Kernel, to determine how far off the estimate is, in a certain iteration, of the target.

The KDE is similar to a histogram, having the same operating principle. However, the data in a KDE overlaps continuously. Depending on the final function or shape obtained, the algorithm determines the loss of the measure, i.e. the difference between the target and the estimation [24], [25].

In this function, the adaptation shows a simpler structure than the original. Only to apply a linear regression via a Mean Square Error (MSE) loss function is needed to determine the accuracy of the estimations, and that can be done with the Python function *MSEloss()*. The loss condition related to the area has been determined to be unnecessary.

2.4.5. Changes in `cnn_utils.py`

The Convolutional Neural Network has a certain number of output channels depending on the dimensions of the system. Hence, the Convolutional Layer that finally generates the output has to be changed to agree to the new size of the system. Accordingly, layer 10 in the code would have to be reshaped in order to output a single channel [26]. This is consistent with the approach taken in first instance, since it was decided to work with images as in DeepSTORM3D.

However, when discussing the code with its creator Elias Nehme, it was observed that it was simpler and a better adaptation of MINFLUX to avoid using images for the learning, i.e. work without convolutions, and instead create a network of linear layers such that with the input of the real emitter positions and photon counts it outputs the fluorophores' location estimates.

3. Further discussion

Many more tests have been carried out than those included in this report (different patterns, methods and their implementations, etc.), but only the most relevant results have been presented, with which it has been seen that the efficiency of the MINFLUX method is very sensitive to the parameters' values and the shape of the beam.

For instance, increasing the simulated number of photons emitted from 100 to 1000 implies an improvement of the CRLB of approximately 14 nm, meaning that localization microscopy can achieve error margins of only from 2 to 4 nm, resolving images at a nanometric scale. Moreover, decreasing L iteratively one could achieve even better resolution. However, this result also implies that, although MINFLUX tries to avoid photobleaching reducing the photon budget, in order to accurately locate the fluorophores in the sample one cannot simply try to drastically decrease the number of emitted photons.

On the other hand, the maximum displacement of the beams' parameter (L), that represents the FOV within which a certain emitter is being exposed, has shown to have certain limitations, as discussed in [section 2.2.2](#). Decreasing the value of L , it is possible to reduce the Standard Deviation of the estimation, but the error starts to increase when it is under 50 nm unaccountably. Besides, neither reducing nor increasing the value of L sharply has a positive impact in the accuracy of localization, because not only it has to be taken into account that the emitter has a certain size and it has to be contained in the area that comprise the different positions of the beam, i.e. the scanning region, but also that firstly one does not know the exact position of the emitter but has to approximate it to set the right FOV, which is easier to do correctly with a large scanning region. On the other hand, if this region is very large, there is a greater chance of sampling more than one emitter at a time which would result in overlapping and thus in a higher error.

When it comes to the size parameter of the donut, $fwhm$, it has been seen that the range in which its value can vary is very narrow, since above 400–500 nm one finds a relatively high STD. It has been noticed that it is a relevant parameter in terms of reducing the area of the PSF, although not by itself. Nonetheless, determining the set of parameters that allow to obtain a better localization while reducing the PSF's footprint is impossible to be done manually.

Another result to discuss is that, as seen, there is no possible way to optimise the shape of the beam or the distribution and number of its different positions manually. One can guess that there will be some other option that has not been considered and enables a more accurate localization microscopy, but to determine which one among all the possible choices is rather impossible.

Consequently, one may think that using Artificial Intelligence (AI) is the best (and only) way to reach the desired objective. That is why the results obtained applying the Deep Learning algorithm are highly relevant.

The DeepSTORM3D code has been changed and adapted to MINFLUX requirements as described, but changing the arrangement of the elements of the microscope and thus placing the phase mask in the path of illumination takes time that has not finally been had, since not only does a new system have to be described and the entire code adapted to it, but also enough information has to be learned to know how to apply these settings.

Furthermore, it would have been impossible to finally generate the learned phase mask and PSF and to analyse the results obtained, because of time constraints. The code has a very high execution time and, besides, the unavoidable step of creating an analytical model to determine the efficiency of the learned PSF in MINFLUX would require of several help and days.

4. Conclusions and perspectives

From the study performed, one can conclude that it is possible to optimise the nowadays methods of Single Molecule Localization Microscopy, and that Artificial Intelligence has a key role in it.

Regular SMLMs reaches around 20 nm of resolution [27]. With MINFLUX, this comes to a few nm while using only low photon counts, which makes it a more useful tool than the traditional methods specially to track molecules.

An analysis of the MINFLUX method has been performed such that one can conclude that it is itself an improvement of SMLM because grants having a better resolution than regular PALM or STORM, while it is possible to further develop the method but only with an AI algorithm, because its complexity and number of free parameters leave no other alternative.

A Deep Learning algorithm developed by Nehme, E. *et al.* [12] comprising 10 different codes with a total of approx. 2200 lines of code has been studied and understood. Despite the difficulty of working with an external code, not programmed by oneself, it has been possible to adapt most of it adequately to the required method. With more time, there is a chance that very important results would have been obtained, expecting, for the learned PSF, a CRLB in MINFLUX below the original one, which already implies very good precisions, and dismissing the problem of overlapping PSFs, hence obtaining a new super resolution technique.

Initially, it would seem that there would be time to carry out the whole project approach. However, during its implementation and partly affected by the consequences of the COVID-19, it has been seen that the study and evaluation of MINFLUX took more time than the expected and, on the other hand, that adapting the DeepSTORM3D code was more difficult than what it was thought and that it required more time than the estimated since it needs a lot of learning effort. Even so, six out of seven specific objectives of this thesis have been successfully met. Although it has not been possible to obtain the learned PSF and an analytic model that allows the computation of the CRLB for MINFLUX with it, the resolution is expected to be of some nanometres below of that of the original method, which would mean that real nanometre resolution would be achieved. However, unfortunately, this is still to be proven.

Some improvements that can be done to this research could be to work with MINFLUX 3D [28]. This way, there would be no need to reduce the dimensions in the Deep Learning code of DeepSTORM3D. Moreover, MINFLUX could be represented in images to fit an algorithm like the latter, the CNN could be used and one would be able to accurately resolve images three-dimensionally.

On the other hand, a different Deep Learning algorithm could be developed which might imply a better performance of the AI and would also represent a deeper integration of

MINFLUX in the code, which would certainly grant that the learned phase mask produces a PSF with a minimum of intensity and that other conditions needed for the right functioning of the technique are fulfilled. Even Machine Learning could be used instead of Deep Learning.

The loss condition for the area could be introduced to see if it betters the resulting accuracy, and for the same purpose one could implement in the DeepSTORM3D algorithm to start the learning from an already specified mask representing a vortex, the one used in MINFLUX, so that the initial illumination is already configured as donut-shaped.

Other possible improvements of the method described could be to introduce in the Deep Learning a certain condition to optimise the distribution of the beam positions to expose the sample, or to generate a MATLAB or Python code that directly computes the CRB when using a certain PSF in MINFLUX only with the 2D or 3D image of that PSF. That way, there would be no need to find an analytical description for it, which would speed up and facilitate the method.

All in all, it has been proven that there is still a long way to go in the field of microscopy, and it is likely that methods that are now understood to be super resolution will become obsolete in the future due to the integration of new techniques such as those studied in this project. This would not only be a breakthrough in photonics but would also lead to great discoveries in the field of medicine.

Bibliography

- [1] “Historical Background of Microscopy.”
<https://www.zeiss.com/microscopy/int/solutions/reference/basic-microscopy/microscopy-historical-perspective.html> (accessed May 06, 2020).
- [2] S. W. Hell, “Microscopy and its focal switch,” *Nat. Methods*, vol. 6, no. 1, pp. 24–32, 2009, doi: 10.1038/nmeth.1291.
- [3] B. Rieger, R. P. J. Nieuwenhuizen, and S. Stallinga, “Computation for nanoscale imaging],” no. January, pp. 49–57, 2015.
- [4] E. Betzig *et al.*, “Imaging intracellular fluorescent proteins at nanometer resolution,” *Science (80-.)*, vol. 313, no. 5793, pp. 1642–1645, Sep. 2006, doi: 10.1126/science.1127344.
- [5] K. Rossmann, “Point spread-function, line spread-function, and modulation transfer function. Tools for the study of imaging systems.,” *Radiology*, vol. 93, no. 2, pp. 257–272, 1969, doi: 10.1148/93.2.257.
- [6] “The Point Spread Function - YouTube.”
https://www.youtube.com/watch?v=Tkc_GOCjx7E (accessed Jun. 10, 2020).
- [7] “Phase mask coded with the superposition of four Zernike polynomials for extending the depth of field in an imaging system | Request PDF.”
https://www.researchgate.net/publication/263549328_Phase_mask_coded_with_the_superposition_of_four_Zernike_polynomials_for_extending_the_depth_of_field_in_an_imaging_system (accessed Jun. 16, 2020).
- [8] <http://csweb.cs.wfu.edu/~pauca/publications/AMOS2002.pdf> (accessed Jun. 16, 2020).
- [9] S. Stallinga and B. Rieger, “Accuracy of the Gaussian Point Spread Function model in 2D localization microscopy,” *Opt. Express*, vol. 18, no. 24, p. 24461, 2010, doi: 10.1364/oe.18.024461.
- [10] E. Nehme, L. E. Weiss, T. Michaeli, and Y. Shechtman, “Deep-STORM: super-resolution single-molecule microscopy by deep learning,” *Optica*, vol. 5, no. 4, p. 458, 2018, doi: 10.1364/optica.5.000458.
- [11] F. Balzarotti *et al.*, “Nanometer resolution imaging and tracking of fluorescent molecules with minimal photon fluxes,” *Science (80-.)*, vol. 355, no. 6325, pp. 606–612, 2017, doi: 10.1126/science.aak9913.
- [12] E. Nehme *et al.*, “DeepSTORM3D: dense three dimensional localization microscopy and point spread function design by deep learning,” 2019, [Online]. Available: <http://arxiv.org/abs/1906.09957>.
- [13] M. Siemons, C. N. Hulleman, R. Ø. Thorsen, C. S. Smith, and S. Stallinga, “High precision wavefront control in point spread function engineering for single emitter localization,” *Opt. Express*, vol. 26, no. 7, p. 8397, 2018, doi: 10.1364/oe.26.008397.
- [14] “Fluorescent Probes | Thermo Fisher Scientific - ES.”
<https://www.thermofisher.com/es/es/home/life-science/protein-biology/protein->

- biology-learning-center/protein-biology-resource-library/pierce-protein-methods/fluorescent-probes.html (accessed Jun. 18, 2020).
- [15] S. Prasad, V. P. Pauca, R. J. Plemmons, T. C. Torgersen, and J. Van Der Gracht, “Pupil-phase optimization for extended-focus, aberration-corrected imaging systems.”
 - [16] S. Prasad, T. C. Torgersen, V. P. Pauca, R. J. Plemmons, and J. Van Der Gracht, “Engineering the Pupil Phase to Improve Image Quality.”
 - [17] “Zernike coefficients.” https://telescope-optics.net/zernike_coefficients.htm#aperture (accessed Jun. 16, 2020).
 - [18] “Zernike polynomials - Wikipedia.” https://en.wikipedia.org/wiki/Zernike_polynomials (accessed Jun. 16, 2020).
 - [19] “Aberraciones de alto orden.” <https://www.vista-laser.com/aberraciones-de-alto-orden/> (accessed Jun. 16, 2020).
 - [20] “Convolutional Neural Networks Definition | DeepAI.” <https://deeptai.org/machine-learning-glossary-and-terms/convolutional-neural-network> (accessed Jun. 16, 2020).
 - [21] “A Comprehensive Guide to Convolutional Neural Networks — the ELI5 way.” <https://towardsdatascience.com/a-comprehensive-guide-to-convolutional-neural-networks-the-eli5-way-3bd2b1164a53> (accessed Jun. 16, 2020).
 - [22] “A Beginner’s Guide to Convolutional Neural Networks (CNNs) | Pathmind.” <https://pathmind.com/wiki/convolutional-network> (accessed Jun. 16, 2020).
 - [23] “GitHub - EliasNehme/DeepSTORM3D: DeepSTORM3D implemented in Pytorch.” <https://github.com/EliasNehme/DeepSTORM3D> (accessed Jun. 15, 2020).
 - [24] “Histograms and kernel density estimation KDE 2 | Biophysics and Beer.” <https://mglerner.github.io/posts/histograms-and-kernel-density-estimation-kde-2.html?p=28> (accessed May 14, 2020).
 - [25] “An introduction to kernel density estimation.” <https://www.mvstat.net/tduong/research/seminars/seminar-2001-05/> (accessed Jun. 19, 2020).
 - [26] “What is PyTorch? — PyTorch Tutorials 1.5.0 documentation.” https://pytorch.org/tutorials/beginner/blitz/tensor_tutorial.html#sphx-glr-beginner-blitz-tensor-tutorial-py (accessed May 20, 2020).
 - [27] “PALM Microscopy, A simple overview.” <https://oni.bio/palm-microscopy> (accessed Jun. 18, 2020).
 - [28] K. C. Gwosch *et al.*, “MINFLUX nanoscopy delivers 3D multicolor nanometer resolution in cells,” *Nat. Methods*, vol. 17, no. 2, pp. 217–224, 2020, doi: 10.1038/s41592-019-0688-0.

Annex

All codes can be found in the following link: <https://github.com/AidaPM/BEP-project.git>